
Article:
Peng, Z. orcid.org/0000-0003-3918-4479, Sonnenwald, F. orcid.org/0000-0002-2822-0406, Smith, C. et al. (3 more authors) (2026) Disaggregation of a tracer cloud in accelerating transitional pipe flow. Journal of Hydraulic Engineering, 152 (1). 04025045. ISSN: 0733-9429

https://doi.org/10.1061/jhend8.hyeng-14271

Disaggregation of a Tracer Cloud in Accelerating Transitional Pipe Flow

Zhangjie Peng[1*], Fred Sonnenwald[2], Colin Smith[3], Jesus Leonardo Corredor Garcia[4], Virginia Stovin[5] and Ian Guymer[6]

[1]Research Associate, School of Mechanical, Aerospace and Civil Engineering, The University of Sheffield, Mappin Street, Sheffield, S1 4DT, United Kingdom. Email: zhangjie.peng@sheffield.ac.uk

[2]Research Data Engineer, IT Services Research & Innovation, The University of Sheffield, Brunswick St, Sheffield, S10 2FN, Sheffield, S3 7RF, United Kingdom. Email: f.sonnenwald@sheffield.ac.uk

[3]Professor in Geotechnical Engineering, School of Mechanical, Aerospace and Civil Engineering, The University of Sheffield, Mappin Street, Sheffield, S1 4DT, United Kingdom. Email: c.c.smith@sheffield.ac.uk

[4]Research Associate, Energy and Environment Institute, The University of Hull, Cottingham Rd, Hull, HU6 7RX, United Kingdom. Email: l.corredor-garcia@hull.ac.uk

[5]Professor of Green Infrastructure for Stormwater Management, School of Mechanical, Aerospace and Civil Engineering, The University of Sheffield, Mappin Street, Sheffield, S1 4DT, United Kingdom. Email: v.stovin@sheffield.ac.uk

[6]Professor of Civil Engineering, School of Mechanical, Aerospace and Civil Engineering, The University of Sheffield, Mappin Street, Sheffield, S1 4DT, United Kingdom. Email: i.guymer@sheffield.ac.uk

* Corresponding author

ABSTRACT

Previous studies on longitudinal solute transport in a pipe during acceleration from laminar to turbulent flow highlighted a disaggregation of the tracer cloud resulting in two peaks occurring downstream from a single pulse injection. It was hypothesised that the disaggregation was caused by the spatially non-uniform acceleration of flow at different radial locations (Hart et al., 2021). This study improves the previous understanding of solute transport during accelerating flow using novel laboratory measurements of pipe cross-sectional tracer distribution from Planar Laser-Induced Fluorescence (PLIF) and radial velocity profiles from an Ultrasonic Velocity Profiler (UVP). Disaggregation of the tracer cloud was observed, with the tracer not being uniformly distributed within the cross-section at the first peak but cross-sectionally well-mixed at the second peak. The relative magnitude of the first peak, compared with the second peak, decreased with the time of injection (and therefore with increased Reynolds number) after the start of the acceleration. Radial velocity profiles showed that the central core of the flow exhibited a smooth, linear increase in velocity compared with the flow closer to the pipe boundary. The data also revealed, for the first time, that the transition time to different flow regimes increased with distance downstream. A model based on the 2D Advection-Dispersion Equation (ADE), parameterised using experimental data, was employed to describe the flow and mixing processes during the acceleration. In addition to the combined effects of the radial velocity profile and radial diffusion coefficient, hypothesised by Hart et al. (2021), this study confirms that it is essential to also include the delay in the transition time at downstream locations to create the observed disaggregation.

PRACTICAL APPLICATIONS

This study revealed the processes underlying the disaggregation observed in tracer concentration profiles during accelerating pipe flows, and it carries significant implications for solute transport, and hence water quality, in water distribution networks. This is particularly the case in remote parts of the water distribution system where unsteady transitional flows are more common due to temporal

variations in demand. This study demonstrates that, in flow accelerating from laminar to turbulent conditions, disaggregation occurs shortly after the contaminant enters the pipe, resulting in a persistent two-peak profile at downstream locations regardless of the flow regime. Accurate estimation of the timing and concentration of these two peaks is crucial for modelling water quality in water distribution networks and premise (building) plumbing systems under low Reynolds number accelerating flow conditions. For the first time, this study provides a mechanistic understanding of the physical processes and outlines a modelling approach suitable to simulate the observed disaggregation.

Keywords: Solute Transport; Accelerating Pipe Flow; Concentration Distribution, Transitional Flow, Radial Diffusion.

INTRODUCTION

Piped water supply systems are characterised by temporal variations in flow, as customer demand varies throughout the day. In remote parts of the system, where demand may be reduced to zero at times, the flow is characterised by accelerations and decelerations, such that the flow transitions between stationary, laminar and turbulent regimes (LeChevallier et al. 2003; Shang et al. 2023). In contrast to the sudden, rapid, changes associated with pipe bursts, these routine, gradual transitions have received little attention in the literature to date.

Transitions between flow regimes are of particular relevance in the context of the transport and mixing of either beneficial or problematic (i.e. contaminant) dissolved material within the flow. In steady laminar conditions, cross-sectional variations in solute concentration will persist over long distances or durations due to limited radial mixing (Flint and Eisenklam 1969; Fowler and Brown 1943; Hart et al. 2016; Keyes 1955; Taylor 1953, 1954a), such that the quantity of a dissolved substance delivered to a customer may depend on the exact position of the draw-off point relative to the supply pipe's perimeter. As a result of the low radial mixing under laminar flow conditions, modelling the diffusive process remains essential for accurately estimating downstream solute concentrations

70 (Basha and Malaeb 2007; Piazza et al. 2020; Romero-Gomez and Choi 2011). In contrast, material will
71 quickly mix across the whole cross-section under fully turbulent conditions (Hart et al. 2016; Taylor
72 1954b). These phenomena similarly affect the longitudinal dispersion observed downstream from the
73 release of a solute/contaminant pulse.

74 Hart et al. (2021) measured longitudinal variations in temporal solute concentration profiles under a
75 range of unsteady flow conditions, including some characterised by a transition from laminar to
76 turbulent flows. These concentrations were mean cross-sectional values which prevented the spatial
77 variation across the pipe cross-section from being discerned. Longitudinal disaggregation of the tracer
78 cloud was observed during all experiments that included an acceleration from laminar to turbulent
79 conditions. The authors hypothesised that, assuming the tracer was initially cross-sectionally well-
80 mixed in the pipe, the tracer in the centre of the pipe would accelerate more than the tracer near the
81 pipe boundary. With little radial exchange under a laminar flow regime, the tracer cloud disaggregates,
82 resulting in the central core tracer arriving at a downstream location ahead of the near-wall tracer.

83 Whilst the Hart et al. (2021) investigation did not include velocity measurements to support their
84 hypothesis, published velocity measurements corresponding to accelerating flows do support it.
85 During the transition to turbulent flow, delays in the response to turbulence production, turbulent
86 energy redistribution, and radial turbulence propagation have been observed (Greenblatt and Moss
87 2004; He and Jackson 2000; Jung and Kim 2017). These delays result in the transition Reynolds number
88 being higher in accelerating flow than in steady flow conditions (Annus and Koppel 2011; Greenblatt
89 and Moss 2004; He and Jackson 2000; Iguchi et al. 2010; Lefebvre and White 1989). The implication
90 of this higher transition Reynolds number for solute transport is that laminar flow conditions persist
91 longer.

92 Kurokawa and Morikawa (1986) measured temporal velocity profiles at different radial locations using
93 a hot wire anemometer. As the flow accelerated from stationary conditions, a point of transition was
94 observed in the temporal velocity profiles. Around this transition, the central core of the flow

exhibited a smooth increase in velocity compared with the flow closer to the pipe boundary. This period of non-equilibrium will clearly impact the solute mixing within the flow and could contribute to tracer disaggregation.

Velocity measurements at multiple longitudinal locations during accelerating flow revealed that the transition time to turbulence increased with the distance from the inlet (Annus and Koppel 2011; Iguchi et al. 2010). This suggests that a non-equilibrium flow regime propagates from upstream to downstream locations, further amplifying the lag effects at downstream locations. Under low acceleration, turbulence is generated near the pipe boundaries close to the inlet and propagates downstream. Intermediate acceleration results in turbulence initially appearing near the pipe entrance and subsequently at downstream locations. For high acceleration, turbulence appears simultaneously near the pipe boundaries along the entire pipe length and propagates radially and axially (Iguchi et al. 2010). Therefore, the occurrence of longitudinally varied transition times is also determined by how quickly the flow velocity increases. Currently, there is no clear definition in the literature on the threshold "low and intermediate acceleration", below which delayed transition times at downstream locations can be observed.

Radial velocity profiles observed in steady flow conditions are smooth, continuous distributions, often described by parabolic or logarithmic functions, whereas during accelerating flows the radial velocity profiles are compound (Greenblatt and Moss 2004; He and Jackson 2000; Iguchi et al. 2010). This discrepancy introduces a further challenge to modelling the flow dynamics during the acceleration.

Existing velocity measurements during accelerating pipe flow provide some insights into the potential causes of solute disaggregation. However, there is no confirmed rule for estimating the transition Reynolds number, transition time along the pipe length, or radial velocity profiles that relate to the acceleration and configuration used in Hart et al. (2021). Additionally, Hart et al. (2021) reported cross-sectionally averaged concentrations rather than cross-sectional concentration distributions, preventing differentiation between tracer concentrations associated with the core and the wall

region. It is clear that concurrent measurements of both radial velocity and full cross-sectional concentration distributions are required to identify the hydrodynamic processes responsible for the solute cloud disaggregation reported in Hart et al. (2021).

This study focuses on the need to understand how the gradual transition from laminar to turbulent flow affects the flow regime and consequent solute mixing within a pipe. The main focus of the paper is on new experimental data, highlighting how, during an acceleration from laminar to turbulent flow conditions: (i) the cross-sectional velocity profile; and (ii) the cross-sectional and longitudinal tracer concentration distributions develop over both time and distance from the injection.

Concentration distributions were measured at four discrete locations and velocity profiles were measured at two discrete locations downstream from the tracer injection. It should be noted that an additional benefit of tracer measurements is that they integrate the hydrodynamic processes occurring throughout the entire reach.

Supported by these measurements, a conceptual model is proposed to describe the key processes associated with a transition from laminar to turbulent flow. In the final part of the paper we present an analytical solution for the conceptual model, parameterised using observed features, to qualitatively verify its ability to describe solute mixing in gradually accelerating pipe flows.

MATERIALS AND METHODS

Experimental Rig

Experiments were conducted on an approximately 13 m long, 2 mm thick, 24 mm internal diameter perspex pipe (Fig. 1(a)). This test section was connected to a recirculating system with a constant head water tank. A perspex plate (inlet in Fig. 1(a)) with an opening of 4.75 mm was placed upstream from the test section to allow better control of the flow rate. Flow control was achieved with a digital butterfly valve located at the downstream end of the test section. The discharge from the pipe was determined using a differential pressure transducer across a 7.0 mm diameter orifice. Tapping points,

11.779 m apart, were used to measure the pipe head loss with a second differential pressure transducer.

Tracer Concentration Measurements

A fluorescent tracer, Rhodamine 6G, was injected into the flow from the pipe wall using a pressurised vessel equipped with a solenoid valve. The injection point was 2.043 m (approximately 85 times the pipe diameter) downstream from the inlet, which is considered to be within the hydrodynamically fully developed region. The pressure vessel maintained a constant pressure of 2.0 bar, and the computer-controlled solenoid valve ensured consistent injected tracer volume and timing. The injection pressure ensured an initial cross-sectionally well-mixed tracer at the injection point (Fig. 1(b), (c) and (d)). Four Planar Laser-Induced Fluorescence (PLIF1 to PLIF4) units were located along the test section to measure the cross-sectional concentration distributions. A full description of the test rig and PLIF units can be found in Peng et al. (2024).

Velocity Measurements

Two 4 MHz Ultrasonic Velocity Profiler (UVP) probes were installed at the location of the first two PLIFs to measure temporal single-component axial velocity profiles (Fig. 1(a)). The UVP probes were installed 19 mm away from the pipe outer wall and at 20° relative to the flow direction, within water baths to reduce multi-phase acoustic reflections. The probes were connected to UVP-DUO (Metflow SA) - an integrated unit for signal generation, data recording and signal processing, and the control of the UVP-DUO was achieved through the UVP software. Although the raw velocity data were recorded at intervals of 0.025 s, the processed data were averaged over 0.25 s to reduce noise. 69 velocity measurements along the UVP probe axis inside the pipe were taken at each time interval and the longitudinal velocity component was used to provide radial velocity profiles.

Due to a small density discrepancy between the seeding particles and water, the particles tend to settle when in contact with water, leading to low quality velocity data near the upper boundary of the

168 pipe. Consequently, only velocity measurements from the bottom half of the pipe were considered
169 for analysis in this study.

170 *Insert Fig. 1.*

171 ## Test Programme

172 Accelerating flow was achieved by opening the digital butterfly valve. Initially, the valve was opened
173 to achieve a design Reynolds Number, R = 1,000 (discharge, Q = 0.0189 l/s; area mean velocity,
174 u = 0.0419 m/s) for 20 seconds to ensure the flow was stable before the acceleration began.
175 Subsequently, the valve was gradually opened in multiple small steps, leading to a linear increase in
176 the Reynolds number to 10,500 (Q = 0.1989 l/s; u = 0.4397 m/s), over 18 s. This acceleration was
177 designed to be similar to the acceleration (from R = 2,700 to R = 47,000 in 60 s) employed by Hart et
178 al. (2021). The flow was maintained at R = 10,500 for a further 30 s until the tracer completely passed
179 all the measurement locations. Tracer injections were made at 0.0 s, 1.0 s, 2.0 s, 3.0 s, 4.0 s, 4.5 s,
180 4.7 s, 5.0 s and 6.0 s from the start of the acceleration, corresponding to design Reynolds numbers of
181 1,000, 1,528, 2,056, 2,583, 3,111, 3,375, 3,481, 3,639 and 4,167. Ten repeats were conducted for each
182 injection time, and all concentration data were logged at a frequency of 100 Hz.

183 Headloss measurements were carried out for several steady flows (700 < R < 11,000) and
184 independently of the concentration measurements to characterise the transition Reynolds number
185 during the accelerating flow, with 10 repeat tests. Headloss was recorded at 100 Hz and averaged over
186 0.5 s intervals. The friction factor, f, was calculated using the Darcy-Weisbach equation (Eq. 1) and
187 the corresponding Reynolds number was calculated from the area mean velocity, u, determined from
188 the measured discharge.

189 $$f = h_f \left(\frac{d}{L}\right)\left(\frac{2g}{u^2}\right) \quad (1)$$

190 where d = pipe diameter; h_f = head loss; L = pipe length; and g = acceleration attributable to gravity.

The temporal velocity measurements were conducted independently of the concentration measurements in two separate series of tests, each consisting of five repeats. The first series measured the velocity profiles at UVP1, 0.834 m downstream of the injection point, while the second series focused on UVP2, positioned 1.7 m downstream of the injection point. During these tests, the velocity was recorded at 40 Hz, the maximum recording frequency achievable with the specific instrument settings for this experiment. To maximise recording resolution and prevent the potential loss of critical information during the accelerating flow due to switching between probes, velocity measurements could not be taken simultaneously at both locations. The boundaries of the pipe were identified based on the physical configuration of the probes. The seeding was 100 µm polyamide, injected at the same location as the tracer. The seeding particle size was selected to maximise the signal reflection and the relative density of the seeding particles is around 1.1, which is close to the water density. To ensure sufficient seeding at the measurement locations before commencing measurements, data collection began 30 s after injection at UVP1 and 1 minute after injection at UVP2.

Uniformity Index

PLIF provides the cross-sectional concentration distribution of the tracer. To quantify the radial concentration distribution, a Uniformity Index (*UI*) for the radial mean concentration distribution was calculated from the corrected and calibrated PLIF images. As described in Peng et al. (2024), the 24 mm diameter pipe area was discretised into 48 concentric circular annuli with 0.25 mm radius increments. For each interval, the radial mean concentration, $c_m(r)$, was calculated. The uniformity of this radial distribution was quantified using a *UI* (Eq. 2), which compares the radial mean concentration profile, $c_m(r)$, with the area mean concentration, $\overline{c_m(r)}$.

$$UI = 1 - \frac{\sum(c_m(r) - \overline{c_m(r)})^2}{\sum c_m(r)^2} \quad (2)$$

For a perfectly uniform concentration distribution, the *UI* is 1.0.

Numerical Model

The conceptual model describing the key processes associated with a transition from laminar to turbulent flow was implemented using a numerical solution to the 2D axisymmetric ADE equation (Eq. 3) (Eftekhari et al. 2015).

$$\frac{\partial c(r,t)}{\partial t} + u(r,t)\frac{\partial c(r,t)}{\partial x} = D_r(t)\left(\frac{1}{r}\frac{\partial c(r,t)}{\partial r} + \frac{\partial^2 c(r,t)}{\partial r^2} + \frac{\partial^2 c(r,t)}{\partial x^2}\right) \quad (3)$$

where $u(r,t)$ and $c(r,t)$ = velocity and concentration at a radial location r and time t and $D_r(t)$ = radial diffusion coefficient. Both the velocity and radial diffusion components in the model were estimated from measured data as follows.

Velocity Profile

The three flow regimes during the accelerating flow were determined from the measured temporal radial velocity profiles (Kurokawa and Morikawa 1986). A power law equation (Eq. 4) was obtained for the laminar and turbulent flow regimes and a time-varying profile was determined for the transitional flow regime.

$$\frac{u(r)}{u_{mean}} = (1 - \left(\frac{2r}{d}\right)^m)^{\frac{1}{n}} \quad (4)$$

where u_{mean} = area mean velocity determined from the measured velocity profile, m and n are empirical parameters.

At any given time during the accelerating flow, the velocity profiles are not the same at different locations, due to the presence of longitudinally different transition times. To maintain the conservation of mass, the absolute values of velocity at different radial locations were scaled. This ensured that the area mean velocity remained constant along the pipe length. Details on the methods of fitting a curve to measured velocity profiles, and the modelled velocity profiles, can be found in Figs. S1-S9 and Tables S1 and S2.

Radial Diffusion

Radial diffusion was assumed to be constant over the pipe radius. Within laminar and transitional flow, radial diffusion was fixed at the molecular diffusion of the tracer (Rhodamine 6G, 4.6×10^{-8} m^2/s). Radial diffusion in turbulent flow ($R \geq 3{,}000$) was estimated by applying Chikwendu's model (Chikwendu 1986) using the temporal tracer area mean concentration profiles under steady flow conditions (Peng et al. 2024) and determined turbulent velocity profiles. From this, the mean flow Reynolds number was used to obtain the corresponding radial diffusion value in the model during the acceleration phase. A comprehensive description of the method used to estimate the area mean radial diffusion coefficient in turbulent flows can be found in Figs. S10-S13.

Temporal Mean Flow and Transition Time

In the conceptual model, the mean flow undergoes linear acceleration from R = 1,100 to R = 10,200 over 18 s, with 5 s of steady flow before and 10 s after the acceleration period to closely mimic the measured acceleration. During the acceleration phase, the flow within the pipe develops through three distinct flow regimes: laminar, transitional, and turbulent.

Two alternative assumptions have been investigated. Model A assumes that the changes between flow regimes occur simultaneously over the entire pipe length (Lefebvre and White 1989), hypothesised by Hart et al. (2021) and here described as a longitudinally uniform transition time. In contrast, Model B assumes that the changes between flow regimes occur at different times longitudinally (Annus and Koppel 2011; Iguchi et al. 2010), described as a longitudinally non-uniform transition time. Both assumptions were tested to evaluate their effects on the modelled flow and mixing dynamics. Under the longitudinally non-uniform transition time assumption (Model B), all three flow states can occur simultaneously at different spatial locations during the acceleration. It was also assumed that the changes between flow regimes only occur during the accelerating phase, and once the acceleration stops, the flow throughout the entire pipe length instantaneously becomes turbulent.

The Advection-Diffusion Equation (ADE) was solved using an existing finite volume MATLAB package (Eftekhari et al. 2015). A time step of 0.0001 s was utilised for a test duration of 25 s. The radial discretisation was 0.1 mm across the 24 mm diameter pipe, while the longitudinal discretisation was 5 mm for the first 6.5 m downstream from the injection location. The selection of these time and spatial steps was determined following discretisation tests, which can be found in Fig. S14 and Table S3. More details on the numerical schemes, mesh-independence tests and order of accuracy, can be found in the supplementary materials. The proposed conceptual model was initially used to simulate the case of an injection made at the start of the acceleration (time 0 s) to explore the ability of the model to describe the observations associated with a transition from laminar to turbulent flow. Further simulations were made for different injection times, to verify the ability of the two different models to describe solute mixing in gradually accelerating pipe flows.

RESULTS AND DISCUSSION

Tracer Concentration Distributions at Different Injection Times

As the measurements are consistent across all ten repeat tests, only one test is presented here. Fig. 2 provides example plots of the temporal variation of the area mean relative concentration profiles derived from the 2D PLIF images for selected injection times. The concentration is non-dimensionalised by the maximum area mean concentration at PLIF1, and the Reynolds number, determined from the measured discharge, is plotted on the secondary Y-axis. In each plot, the vertical red shaded area denotes the injection period, while the horizontal blue shaded area indicates the transitional flow regime as determined by headloss measurements during steady flow conditions.

Fig. 2(a) shows the injection made at t = 0 s (R = 1,093), i.e. the start of the acceleration, corresponding to a laminar flow condition within the pipe. In all the results, the stated Reynolds number corresponds to the measured instantaneous discharge at the start of the injection time. Two peaks were observed in the temporal concentration profiles at all the measurement locations in this test. Fig. 2(b) presents the concentration profiles for the injection at 4 s (R = 3,177) into the acceleration when the mean flow

R was indicative of turbulent flow conditions. Only one peak was recorded at PLIF1, but two peaks were recorded at the three downstream locations; in each case, the first peak had higher concentrations than the second peak. Fig. 2(c), from an injection at 4.7 s (R = 3,644) into the acceleration, shows results similar to the injection at 4 s. Two peaks were recorded at the three downstream locations, but the first peak is now significantly lower than the second (i.e. about 1/3 of the second peak). Fig. 2(d) shows the results for an injection at 6 s (R = 4,706) into the acceleration, where only a single peak was recorded at all four measurement locations. In the tests where the two peaks were recorded, the time difference between the two peaks increases with the distance from the injection (e.g. 1 s at PLIF2 and 3.2 s at PLIF4 for injection at 4.7s), suggesting that the tracer creating the first peak accelerated more than the tracer within the second peak. The peak concentration decreases with distance, and the spread of the concentration profiles increases accordingly. The distribution around the second peak shows a greater spread than the first, which suggests greater longitudinal mixing. As stated previously, disaggregation of a single peak distribution was first observed by Hart et al. (2021). Their rig did not have a diaphragm plate, yet similar area mean concentration distributions were observed.

Insert Fig. 2.

Fig. 1b shows the well-mixed cross-sectional concentration distribution produced at the injection location. In Fig. 1d, 0.5 s after the start of the injection, the effect of longitudinal differential advection can be seen on the leading edge of the tracer pulse, creating the non-uniform cross-sectional distribution shortly afterwards at PLIF1. Figs. 3 & 4 present selected concentration profiles and *UI* values (Eq. 2) associated with injections at t = 6.0 s, R = 4,706 (Fig. 2(d)) and t = 4.0 s, R = 3,177 (Fig. 2(b)) respectively. These cases correspond to injections performed when the flow was fully turbulent and undergoing transition respectively. In each case subplot (a) presents the cross-sectional concentration distributions and subplot (b) presents the *UI* values superimposed on the area-mean concentration profiles. In situations where the longitudinal concentration profile exhibited a single peak, the cross-sectional concentration profiles shown in (a) represent times before, at and after the

peak. The timings are indicated by vertical dashed lines in (b). Where two peaks were observed, the sampled slices correspond to the first peak, an intermediate time and the second peak.

Fig. 3 illustrates the tracer distribution and uniformity index for the more straightforward case, i.e. an injection at 6.0 s, R = 4,706 when the flow is fully turbulent. At PLIF1, some instability is observed, with the tracer not cross-sectionally uniformly distributed and displaying some random patterns in the tracer distributions. However, at all downstream locations, the tracer is well-mixed throughout the test. The uniformity index at all measurement locations confirms cross-sectionally well-mixed concentrations at the peak area mean concentrations. These observations are, as expected, similar to the tracer behaviour under steady turbulent flow conditions shown in Peng et al. (2024).

Insert Fig. 3

Fig. 4(a) illustrates the tracer distribution over the pipe cross-section at selected times at the four measurement locations during the accelerating flow for the injection at 4.2 s, R = 3,513. At PLIF1, at 7.67 s, before the peak area mean concentration, most of the tracer is located at the centre of the pipe. At the peak area mean concentration, 7.97 s, the concentration distribution is non-uniform. However, at 10.45 s, when most of the tracer has passed this measurement location, a more uniform cross-sectional distribution is evident. At PLIF2, at 10.44 s, coinciding with the first peak of the area mean concentration profile and with the third selected time for PLIF1, the distribution is highly non-uniform compared with the well mixed profile evident at PLIF1 at the same point in time. This confirms different flow conditions at the two measurement locations existing at the same time. At 11.45 s, corresponding to the second peak of the area mean concentration, a uniform distribution of tracer is seen. At PLIF3, the concentrations recorded at the first peak are not uniformly distributed, while the second peak shows a uniform distribution. At PLIF4, the tracer is uniformly distributed, i.e. well-mixed, at all selected times.

Insert Fig. 4

Fig. 5 presents the temporal variation of the area mean concentration profiles at the four measurement locations for all injection times examined in this study. The concentration is normalised by the peak concentration measured at each location, and the time is plotted relative to the first arrival time. At PLIF1 two peaks only arise when the injection occurs before 4.0 s from the start of the acceleration (R = 3,177), and the second peaks are less distinct compared with downstream locations. At all downstream locations, two peaks are observed for injections made earlier than 6.0 s, R = 4,706. This transition from double to single peak is indicated by the dashed red line in Fig. 5. Visually, the time difference between the two peaks increases with distance downstream but decreases with time of injection after the start of the acceleration. When the injection occurs at early stages of acceleration, the first peak exceeds the second, but as injection time increases, the first peak diminishes.

Insert Fig. 5

Fig. 6 illustrates the *UI* of the tracer at the area mean concentration peaks for all tests. Fig. 6(a) displays the *UI* for the first peak, while Fig. 6(b) shows the *UI* for the second peak. At upstream locations (PLIF1 to PLIF3), the second peak consistently exhibits more uniform distributions than the first peak, while at the downstream location (PLIF4), concentration distributions at both peaks are consistently uniform (i.e. *UI* close to 1.0). Across all measurement locations, the *UI* increases with injection time for both peaks (i.e. from 0.6 to close to 1.0 for the first peak and from 0.8 to close to 1.0 for the second peak). Longitudinally, the *UI* for the first peak decreases with distance at the first three measurement locations, whereas for the second peak, the *UI* increases with distance. This suggests that the fluid in the pipe centre is rapidly accelerating, with little radial mixing, between PLIF1 and PLIF3, leading to the tracer from the pipe core being less well-mixed at downstream locations. This is confirmed by the results presented in Fig. 4.

Insert Fig. 6

In summary, concentration measurements conducted during accelerating flow for different injection times revealed the presence of two peaks in the temporal area mean concentration when injections occurred during the initial stages of acceleration, that is before 6 s. Notably, at comparable acceleration stages, the tracer exhibited different distributions at different longitudinal positions. As the injection time increased, the first peak gradually diminished compared to the second peak. Moreover, it was consistently observed that the first peaks exhibited less uniform cross-sectional distributions compared with the second peaks. The concentration measurements highlight the complex hydrodynamics associated with accelerating transitional flows.

Transition Reynolds Number During Accelerating Flow

Fig. 7 displays the friction factor computed from headloss and discharge measurements obtained during both steady and accelerating flows across the 10 repeat tests. For the accelerating flow tests, standard deviations are included to characterise the uncertainties associated with the estimates of both Reynolds number and the friction factor. Minor fluctuations in the Reynolds number suggest good repeatability of the flow conditions across the tests. However, a more pronounced difference is observed in the friction factor, attributed to pressure instability during acceleration. The discontinuities in the data indicate flow regime transitions. It may be seen that, during the acceleration, laminar flow occurs at $R < 2{,}500$, while turbulent flow occurs at $R > 3{,}900$ (shaded red area). In contrast, the transition Reynolds numbers determined under steady flow conditions ($R = 2{,}300$ and $R = 2{,}800$) were clearly lower. The need for higher Reynolds numbers to drive the transition to turbulence during acceleration is caused by the delay in turbulence production, energy redistribution, and radial propagation of turbulence (Greenblatt and Moss 2004; He and Jackson 2000; Jung and Kim 2017).

Insert Fig. 7.

Further detailed information regarding the radial and longitudinal flow dynamics is required to fully explain the observed variations in cross-sectional mixing and longitudinal concentration profile

385 shapes. However, the discrepancy between the turbulent transition Reynolds number determined
386 during the accelerating flow and steady flow conditions suggests that laminar flow conditions can last
387 for longer in accelerating flow and therefore amplify the differential velocity effect on longitudinal
388 dispersion. Further confirmation is provided in Fig. 4 which shows that at 10.5 s after the acceleration
389 started, i.e. R > 7,000, when conditions are fully turbulent according to the accelerating data presented
390 in Fig. 7, the tracer concentrations exhibited clear transitional behaviour, with the early parts of the
391 trace showing non-uniform cross-sectional distributions (PLIF2 and PLIF3).

392 ## Measured Velocity Profile

393 The integrated area mean velocity was determined by integrating the radial distribution of the axial
394 velocity across the pipe cross-section, while the mean velocity was obtained by dividing the orifice
395 derived discharge by the cross-sectional pipe area. Fig. 8(a) compares these three estimates, and good
396 agreement between the measurements confirms the reliability of the UVP measurements. During the
397 steady state and low-velocity flow phase, minimal velocity fluctuations were observed, while greater
398 fluctuations occurred during the high-velocity and final steady flow conditions. This degree of
399 fluctuation is indicative of the transition to a different flow regime. At UVP1, velocity fluctuations
400 become significant after 9 s, indicating a transition to turbulent flow, while at UVP2, noticeable
401 velocity fluctuations are observed after approximately 11 s, suggesting a delayed transition to
402 turbulent flow.

403 Fig. 8(b) displays one of the five replicate temporal velocity profiles for selected radial locations during
404 the accelerating flow at UVP1. Consistent with the findings of Kurokawa and Morikawa (1986) for a
405 low acceleration, there is a stage where the velocity near the pipe boundary stops accelerating, while
406 the velocity at the pipe centre continues to accelerate. The time when the velocity near the pipe
407 boundary begins to remain constant defines the start of the transition from laminar flow to turbulent
408 flow. At the end of the transition phase, velocities at all radial locations change rapidly, with the
409 velocity at the pipe boundary increasing and the velocity at the pipe centre decreasing. This rapid

change defines the end of the transition to turbulent flow (Kurokawa and Morikawa, 1986). At UVP1, these two transition times were found to be at 6 s and 9 s, respectively. Additional details on the determination of the transition times can be found in Fig. S1.

Fig. 8(c) illustrates the velocity profiles at UVP2, where a similar pattern is observed. However, consistent with some previous studies (Annus and Koppel 2011; Iguchi et al. 2010), the switches to transitional flow and turbulent flow occur at later times at this location (at 8 s and 11 s) compared to UVP1. This delayed longitudinal transition time at downstream locations is also evident in the concentration measurement, where the tracer exhibits a uniform distribution at the upstream location but not at the downstream location at the same time (Fig. 4).

At both measurement locations, during the transitional flow, a unique velocity profile is observed, characterised by a constant velocity close to the pipe boundary. This velocity profile results in the tracer near the pipe boundary travelling at a much lower speed than the tracer in the centre, leading to the formation of two peaks in the concentration profiles.

The radial velocity profile within the same flow regime during the accelerating flow was found to have a similar shape independent of longitudinal location (Figs. S2-S4). Fig. 8(d) is an example of non-dimensionalised velocity data for laminar flow at UVP1, Fig. 8(e) is for transitional flow and Fig. 8(f) is for turbulent flow in the same test.

Insert Fig. 8.

Velocity Profile Parameterisation

The parameters m and n in the power law equation (Eq. 4) were calibrated to fit the measured velocity data in the five repeat tests at the two locations for the laminar, transitional and turbulent flow regimes. Mean values of m and n (Table 1) were obtained for all the tests. Fig. 8(d), 8(e) and 8(f) compare measurements with fitted models and show good agreement. More details on the curve fitting and calibrated parameters can be found in Figs. S2-S4 and Tables S1 and S2.

Transition Time Parameterisation

Head loss measurements during the accelerating flow suggested that the transition to transitional flow is at R = 2,500 and the transition to turbulent flow is at R = 3,900 (Fig. 7). Assuming that the entire pipe length transitions to a different flow regime simultaneously, Model A, Fig. 9(a) shows the development of the flow regimes in the first 6.0 m of the pipe.

However, the data presented in Fig. 8 clearly points to a delay in the transition at the downstream measurement location. Based on the time corresponding to the transition times in Fig. 8(b) and (c) and the distance between UVP1 and UVP2, linear equations were derived to establish the relationship between the transition times and distance. Fig. 9(b) illustrates the estimated transition times corresponding to the imposed acceleration (dash-dotted line on the secondary y-axis) under the assumption of longitudinally non-uniform transition time, Model B. The vertical transition at 18 s in Fig. 9(b) indicates that the flow throughout the entire pipe length shifts to turbulent flow instantaneously once the acceleration stops. A detailed description of the determination of transition times at different longitudinal locations can be found in Fig. S7.

Insert Fig. 9.

Model Results

Fig. 10 compares the model results and the experimental measurements at the four PLIF locations for the case of tracer injection made at time 0.0 s, R = 1,093. The area mean temporal concentration profiles and the Uniformity Index (*UI*) are used to evaluate the model results.

From Model A, with the longitudinally uniform transition time (second column in Fig. 10), the simulations exhibit two peaks in the area mean concentration profiles at the first measurement location PLIF1, X = 0.834 m. At the three downstream locations (PLIF2, 3 & 4, X = 1.702, X = 3.222 & 5.529 m), only a single peak is simulated. Model A does not, therefore, reflect the observed data (first column).

458 In contrast, Model B (third column in Fig. 10), with the inclusion of longitudinally non-uniform
459 transition times, resulted in the simulation of two peaks in the area mean concentration profiles at all
460 PLIF locations, as observed in the experimental data. Model B also shows the second peaks to be cross-
461 sectionally well-mixed at the two downstream locations. Model B correctly reproduces both the
462 observed disaggregation and the cross-sectional mixing characteristics at the two peaks.

463 Nonetheless, there are some discrepancies between the simulation results using Model B and the
464 experimental data. The modelled spread of the first peak is less than the measurements during
465 laminar and transitional flow regimes, suggesting that the radial diffusion may differ from the assumed
466 value of molecular diffusion. This is especially so during the transitional flow regime, where the high-
467 velocity gradient between the pipe core and flow adjacent to the pipe boundary is likely to introduce
468 more radial mixing than molecular diffusion. Additionally, the timing of the two peaks in the simulation
469 shows some discrepancy with the measurements, which could be attributed to the limitation in
470 determining the transition times between different flow regimes. Further exploration of these
471 hypotheses requires higher temporal resolution velocity measurements that are not feasible with the
472 current UVP velocity measurements.

473 Based on the simulation results, it can be concluded that transitional velocity profiles, longitudinally
474 non-uniform transition times and radial diffusion in turbulent flows contribute to the observed mixing
475 characteristics during accelerating flow. The presence of two peaks is primarily caused by the unique
476 velocity profile associated with the transitional flow regime, where the tracer at the pipe core
477 accelerates more rapidly than the tracer at the pipe boundary. This finding, illustrated by Model A, is
478 consistent with the hypothesis proposed in Hart et al. (2021). However, to simulate the two peaks at
479 downstream locations, a longitudinally non-uniform transition time needs to be considered, as in
480 Model B, to prolong the duration of the transitional flow regime along the length of the pipe.
481 Furthermore, the cross-sectional tracer distribution is predominantly influenced by radial diffusion.
482 Incorporating radial turbulent diffusion into the model during the turbulent flow regime creates the

observed cross-sectional uniform distributions observed in the second peaks at downstream locations. These features match the experimental measurements.

Insert Fig. 10.

The onset of instability caused by shear stress near the pipe wall during acceleration is not simultaneous throughout the pipe. Instead, it propagates from upstream to downstream, significantly influencing the mixing processes. Fig. 11 highlights the processes identified during the accelerating flow showing the modelled velocity, radial concentration distribution, and radial sum concentration at 11.8 s since injection between 0.5 m and 4.0 m downstream from the injection point using Model B. At this point in time, the mean flow is turbulent (R = 7,066) and three distinct flow regimes occur along the pipe: a laminar flow velocity profile at the downstream end (beyond 3.35 m), a transitional flow velocity profile in the middle section (between 2.05 m and 3.35 m), and a turbulent flow profile upstream (from 0 m to 2.05 m). The transitional flow regime drives the separation of the tracer cloud, while the two orders of magnitude higher radial diffusion in the turbulent flow regime moves the tracer near the pipe boundary toward the pipe centre, resulting in a well-mixed cross-sectional distribution at the second peak. In contrast, the limited radial mixing in the laminar and transitional flow regimes keep the tracer at the pipe core, resulting in a cross-sectionally not well-mixed condition at the first distribution peak of the tracer. An animation of the model output is provided in Video S1 and Peng et al. (2025).

Insert Fig. 11.

Model Verification

The concentration measurements from later injection times provide an opportunity to further confirm the applicability of Model B. Simulations were carried out with Model B for injections at different times, and the results for the two downstream locations (PLIF3 & PLIF4) are presented in Fig. 12. These downstream locations were chosen due to their suitability for observing the effects of the processes, which become more noticeable over time and distance compared to the upstream locations. The

observed change in the relative concentration of the two peaks at the downstream locations with injection time mirrors the experimental measurements shown in Fig. 5. Specifically, as the injection is made at later times during the acceleration, the first peak concentration decreases relative to the second peak. In addition, the uniformity index at the two peaks also matches the experiments, where the second peak is always more uniformly distributed than the first peak. However, in Fig. 5, it was noted that the first injection time to show a reduced first peak compared with the second peak was 4.7 s, R = 3,644, whereas in conceptual Model B, the transition occurred at an injection time of 4.0 s (Fig. 12c). The limited spread of tracer around the first peak again suggests that the radial diffusion coefficient for non-turbulent flow conditions may be underestimated. Despite this small difference, the overall similarity demonstrates that the processes integrated into Model B closely represent the hydraulics and mixing characteristics during accelerating transitional pipe flow.

Insert Fig. 12.

CONCLUSIONS

Experimental studies of solute transport in accelerating pipe flows were conducted to understand how the gradual transition from laminar to turbulent flow affects the flow regime and consequent solute mixing within a section of straight pipe. Four Planar Laser-Induced Fluorescence (PLIF) units were used to measure cross-sectional tracer concentration distributions corresponding to a pulse of tracer introduced into the flow at different times during the acceleration. Disaggregation of the tracer cloud was observed when the tracer was injected at an early stage of the acceleration. The relative concentration of the first peak compared with the second peak reduced with increased time of injection after the start of the acceleration. The spatial uniformity of the tracer shows that the first peak is not cross-sectionally well-mixed at the upstream locations while the second peak is cross-sectionally well-mixed at all locations.

Headloss measurements during the accelerating flow demonstrated that the transition to a different flow regime occurs at a higher Reynolds number than for steady flow conditions. Radial velocity

measurements with an Ultrasonic Velocity Profiler (UVP) at two longitudinal locations during the accelerating flow showed that the central core of the flow exhibits a smooth linear increase in velocity compared with the flow closer to the pipe boundary. In addition, it was demonstrated that the transition time to a different flow regime increased with distance downstream.

Supported by laboratory measurements, a model based on the 2D axisymmetric Advection-Dispersion Equation (ADE) was able to describe the key mixing processes associated with a transition from laminar to turbulent flow. The velocity and the radial diffusion components in the model were estimated from the measured data. It was shown that disaggregation can be successfully represented by including appropriate velocity profiles for the different flow regimes and incorporating suitable magnitudes of turbulent diffusion (Model A). However, to fully describe the disaggregation, with the non-uniform cross-sectional distribution of tracer, this study has demonstrated for the first time that it is essential to include the effects of longitudinal non-uniform transition time (Model B).

DATA AVAILABILITY STATEMENT

Some or all data, models, and code generated or used during the study are available in a repository or online in accordance with funder data retention policies from Peng et al. (2025), DOI: 10.15131/shef.data.26266174.

ACKNOWLEDGEMENTS

The authors would like to thank Joseph Milner, who provided technical support for all the laboratory studies conducted at the University of Sheffield. Additional appreciation was also given to Professor Shuisheng He and Oliver Cooper for their generous provision and assistance in using their lab space. This work was supported by the EPSRC Grant No. EP/P012027/1.

SUPPLEMENTARY MATERIALS

Figs. S1-S14, Table S1-S3, and Video S1 are available online in the ASCE Library (ascelibrary.org).

REFERENCES

Annus, I., and Koppel, T. (2011). "Transition to turbulence in accelerating pipe flow." *Journal of Fluids Engineering, Transactions of the ASME*, 133(7).

Basha, H. A., and Malaeb, L. N. (2007). "Eulerian–Lagrangian Method for Constituent Transport in Water Distribution Networks." *Journal of Hydraulic Engineering*, 133(10), 1155–1166.

Chikwendu, S. C. (1986). "Calculation of longitudinal shear dispersivity using an N-zone model as N → ∞." *Journal of Fluid Mechanics*, 167(1), 19.

Eftekhari, A. A., Schüller, K., Planella, F. B., Werts, M., and Hosseinzadeh, B. (2015). "FVTool: a finite volume toolbox for Matlab." *Zenodo*, <https://doi.org/10.5281/zenodo.32745>.

Flint, L. F., and Eisenklam, P. (1969). "Longitudinal gas dispersion in transitional and turbulent flow through a straight tube." *The Canadian Journal of Chemical Engineering*, John Wiley & Sons, Ltd, 47(2), 101–106.

Fowler, F. C., and Brown, G. G. (1943). *Contamination by Successive Flow in Pipe Lines*. American institute of chemical engineers.

Greenblatt, D., and Moss, E. A. (2004). "Rapid temporal acceleration of a turbulent pipe flow." *Journal of Fluid Mechanics*, Cambridge University Press, 514, 65–75.

Hart, J. R., Guymer, I., Sonnenwald, F., and Stovin, V. R. (2016). "Residence Time Distributions for Turbulent, Critical, and Laminar Pipe Flow." *Journal of Hydraulic Engineering*, 142(9), 1–10.

Hart, J., Sonnenwald, F., Stovin, V., and Guymer, I. (2021). "Longitudinal Dispersion in Unsteady Pipe Flows." *Journal of Hydraulic Engineering*, 147(9), 1–12.

He, S., and Jackson, J. D. (2000). "A study of turbulence under conditions of transient flow in a pipe." *Journal of Fluid Mechanics*, Cambridge University Press, 408, 1–38.

Iguchi, M., Nishihara, K., Nakahata, Y., and Knisely, C. W. (2010). "Effect of initial constant

acceleration on the transition to turbulence in transient circular pipe flow." *Journal of Fluids Engineering, Transactions of the ASME*, 132(11), 1112031–1112039.

Jung, S. Y., and Kim, K. (2017). "Transient behaviors of wall turbulence in temporally accelerating channel flows." *International Journal of Heat and Fluid Flow*, Elsevier Inc., 67, 13–26.

Keyes, J. J. (1955). "Diffusional film characteristics in turbulent flow: Dynamic response method." *AIChE Journal*, John Wiley & Sons, Ltd, 1(3), 305–311.

Kurokawa, J., and Morikawa, M. (1986). "Accelerated and Decelerated Flows in a Circular Pipe : 1st Report, Velocity Profile and Friction Coefficient." *Bulletin of JSME*, The Japan Society of Mechanical Engineers, 29(249), 758–765.

LeChevallier, M. W., Gullick, R. W., Karim, M. R., Friedman, M., and Funk, J. E. (2003). "The potential for health risks from intrusion of contaminants into the distribution system from pressure transients." *Journal of Water and Health*, IWA Publishing, 1(1), 3–14.

Lefebvre, P. J., and White, F. M. (1989). "Experiments on transition to turbulence in constant-acceleration pipe flow." *Journal of Fluids Engineering*, 111(December), 1–5.

Peng, Z., Stovin, V., and Guymer, I. (2024). "Radial Mixing in Steady and Accelerating Pipe Flows." *Journal of Hydraulic Engineering*, 150(6).

Peng, Z., Sonnenwald, F., Smith, C., Corredor Garcia, JL., Stovin, V., and Guymer, I. (2025). "Dataset for cross-sectional solute concentration and velocity distribution with headloss in transitional accelerating pipe flows. " Sheffield, UK: Univ. of Sheffield.

Piazza, S., Mirjam Blokker, E. J., Freni, G., Puleo, V., and Sambito, M. (2020). "Impact of diffusion and dispersion of contaminants in water distribution networks modelling and monitoring." *Water Supply*, IWA Publishing, 20(1), 46–58.

Romero-Gomez, P., and Choi, C. Y. (2011). "Axial Dispersion Coefficients in Laminar Flows of Water-Distribution Systems." *Journal of Hydraulic Engineering*, American Society of Civil Engineers, 137(11), 1500–1508.

Shang, F., Burkhardt, J. B., and Murray, R. (2023). "Random Walk Particle Tracking to Model

607 Dispersion in Steady Laminar and Turbulent Pipe Flow.” *Journal of Hydraulic Engineering*,
608 149(7), 1–9.
609 Taylor, G. I. (1953). “Dispersion of soluble matter in solvent flowing slowly through a tube.”
610 *Proceedings of the Royal Society of London. Series A. Mathematical and Physical Sciences*,
611 219(1137), 186–203.
612 Taylor, G. I. (1954a). “Diffusion and mass transport in tubes.” *Proceedings of the Physical Society.*
613 *Section B*, 67(12), 857–869.
614 Taylor, G. I. (1954b). “The dispersion of matter in turbulent flow through a pipe.” *Proceedings of the*
615 *Royal Society of London. Series A. Mathematical and Physical Sciences*, The Royal Society
616 London, 223(1155), 446–468.

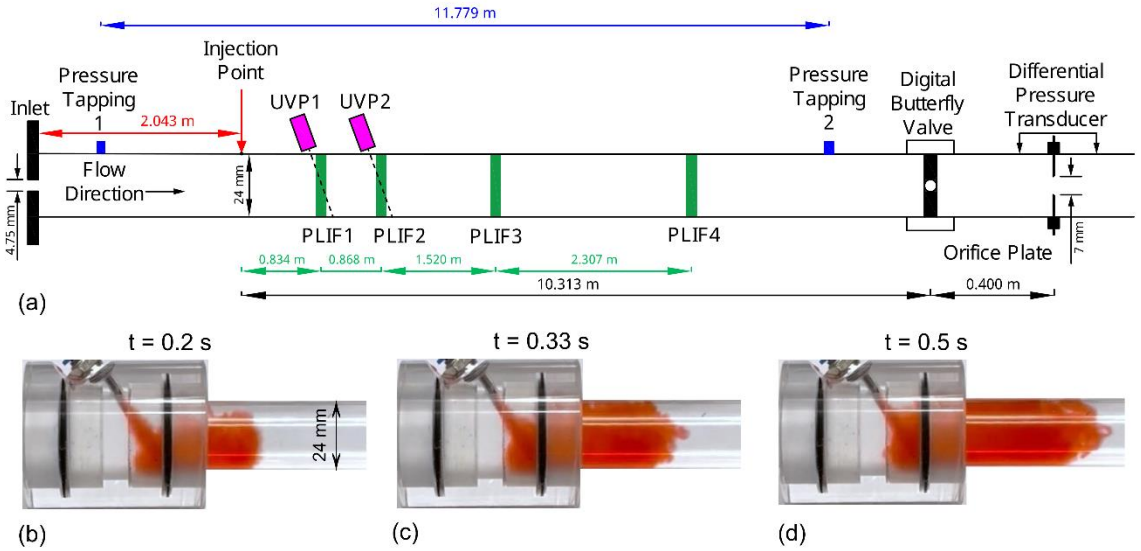

Fig. 1. Experimental set-up and instrumentation: (a) pipe test section (not to scale); (b), (c) and (d) photographs of food dye injection.

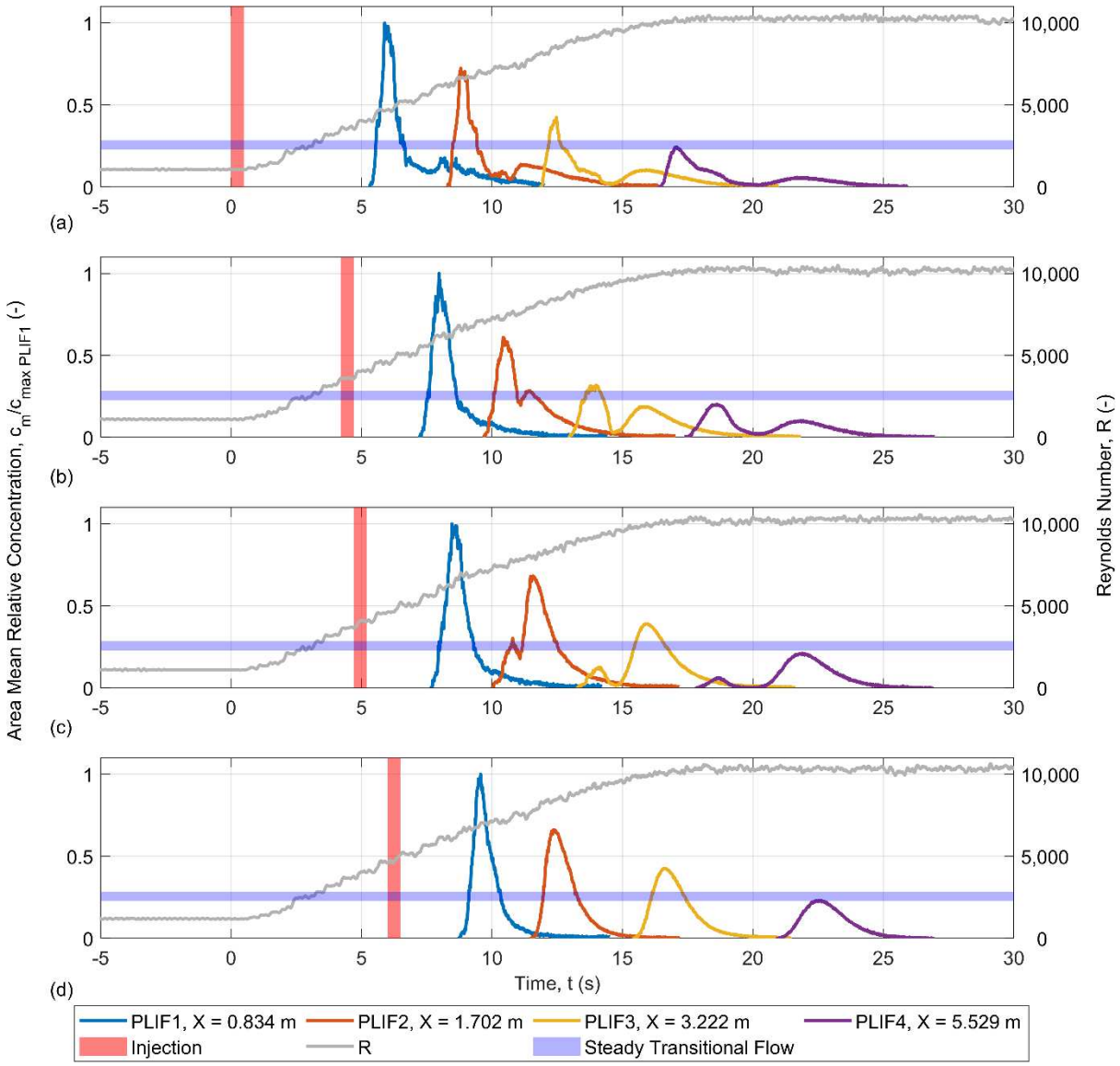

Fig. 2. Area mean temporal concentration profiles from 2D PLIF images in accelerating flow with tracer injections made at different times after the start of acceleration; (a) 0.0 s, R = 1,093; (b) 4.2 s, R = 3,513; (c) 4.7 s, R = 3,644; (d) 6.0 s, R = 4,706.

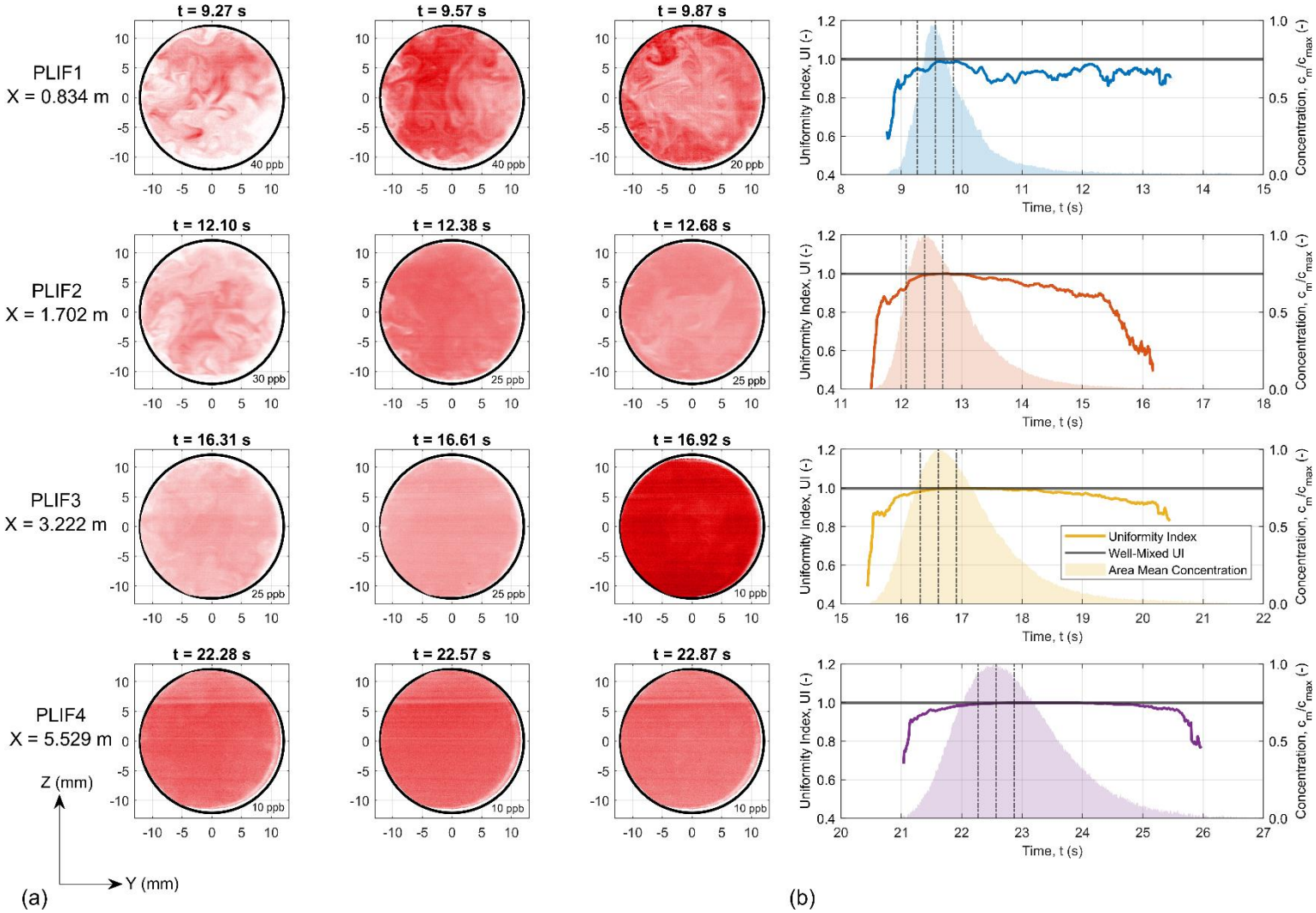

Fig. 3. Accelerating flow with injection at Time = 6.0 s, R = 4,706; (a) cross-sectional concentration distribution for selected times (the maximum concentration of the distribution is indicated at the bottom right corner); (b) temporal uniformity index profiles derived from PLIF images, the vertical lines correspond to the selected time in Fig. 3 (a).

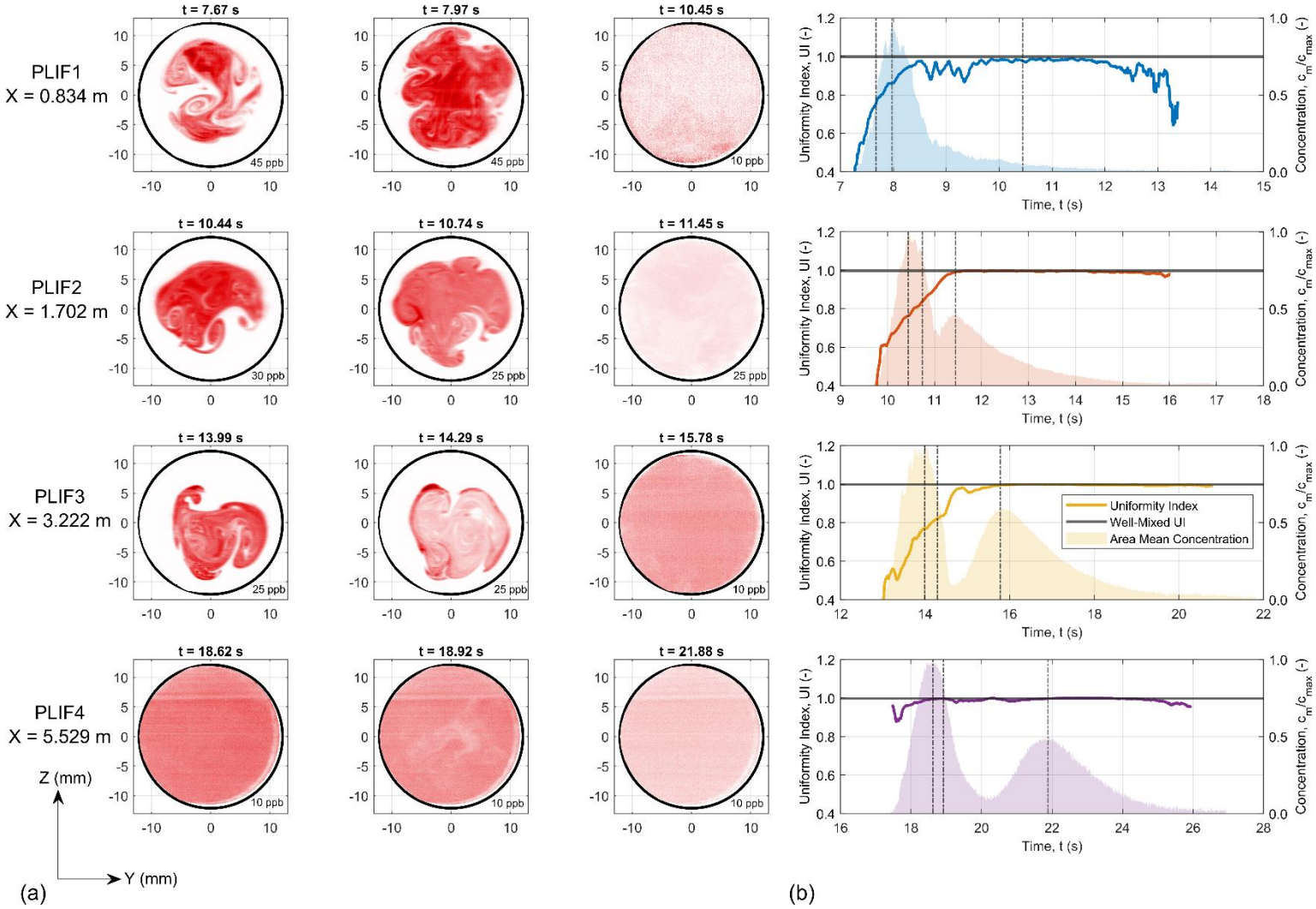

Fig. 4. Accelerating flow with injection at Time = 4.2 s, R = 3,513; (a) cross-sectional concentration distribution for selected times (the maximum concentration of the distribution is indicated at the bottom right corner); (b) temporal uniformity index profiles derived from PLIF images, the vertical lines correspond to the selected time in Fig. 4 (a).

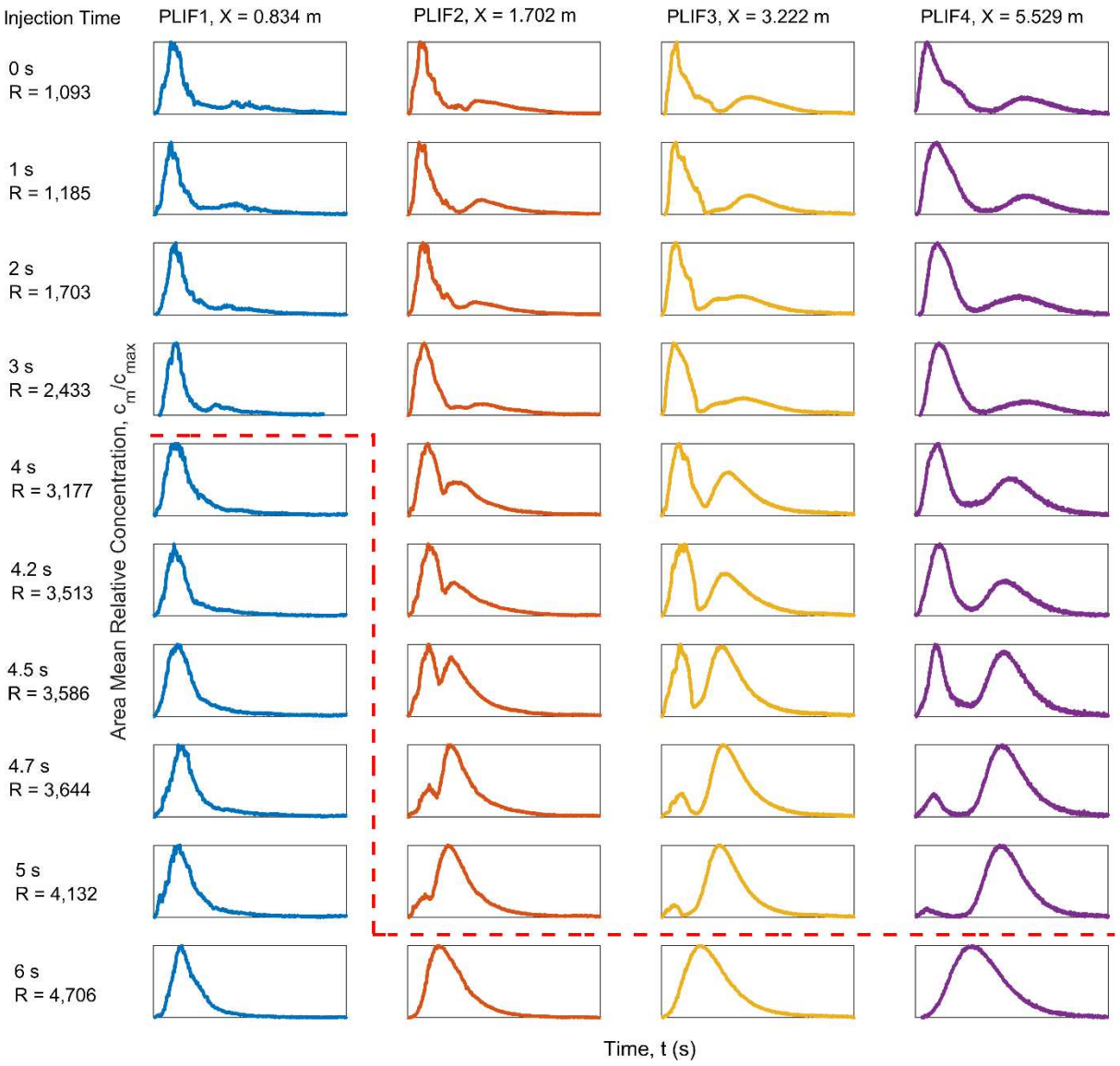

Fig. 5. Temporal area mean concentration profiles from 2D PLIF images at different injection times.

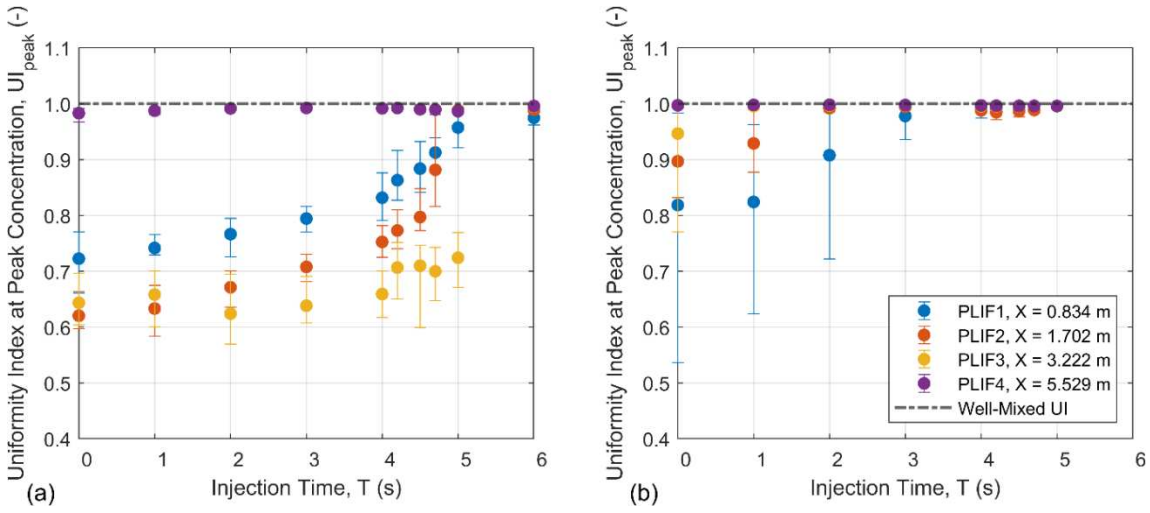

Fig. 6. Uniformity index for peak concentrations at: (a) first peak; (b) second peak.

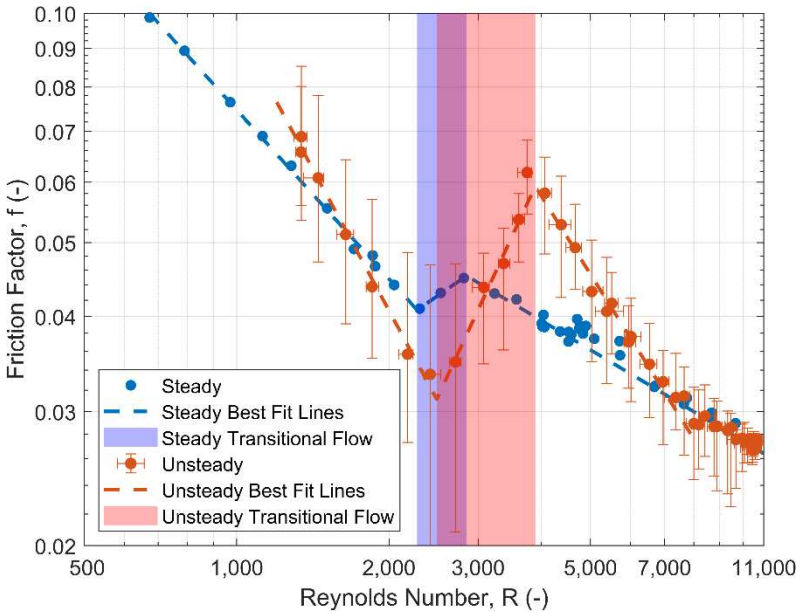

Fig. 7. Variation of friction factor with Reynolds number under steady and accelerating flow conditions.

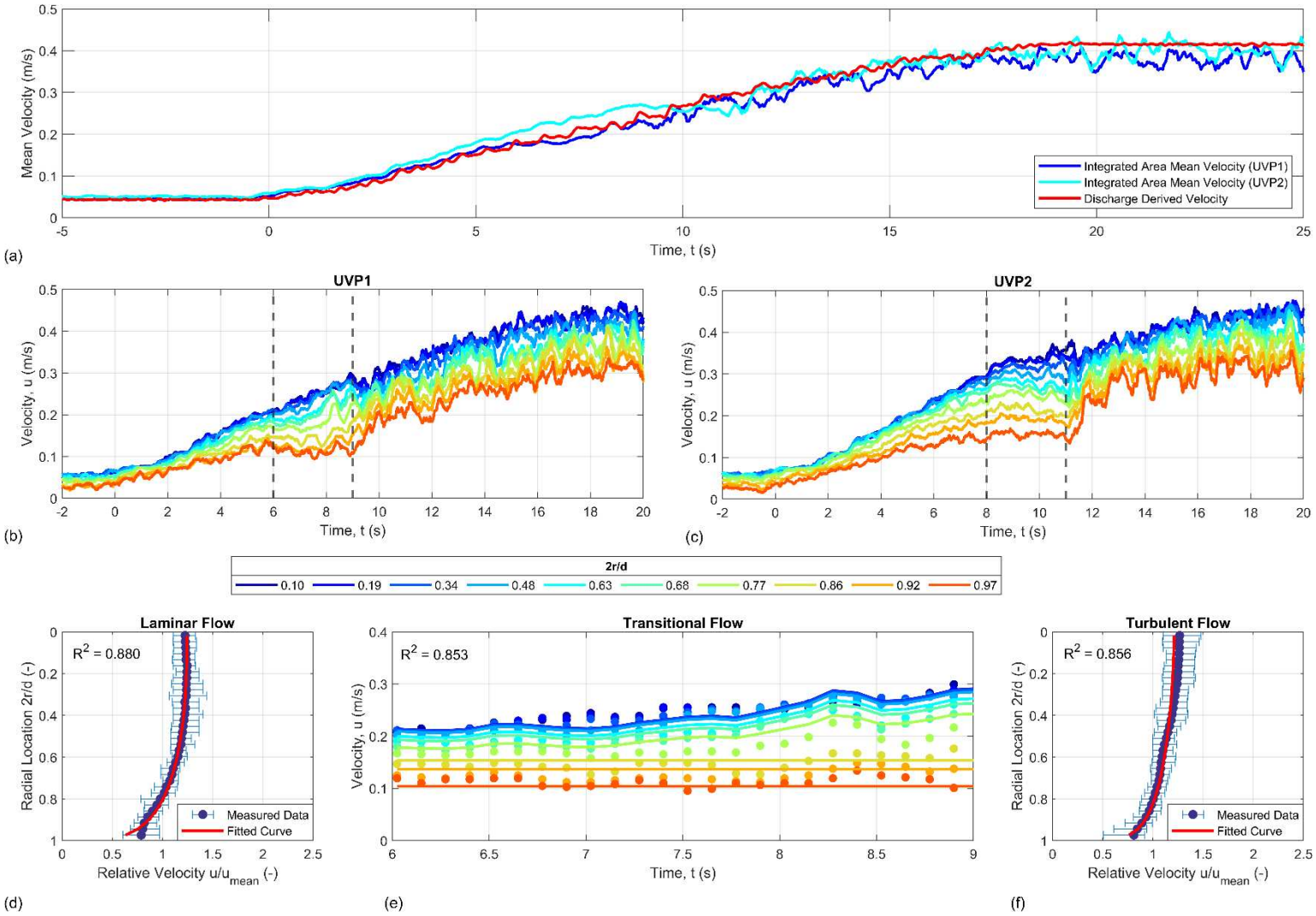

Fig. 8. UVP measured velocity during the accelerating flow; (a) UVP integrated velocity and discharge determined velocity; temporal velocity profiles at different radial locations measured at (b) UVP1 and (c) UVP2 (the two dashed vertical lines show the transition times); Measured velocity data and fitted curve at UVP1 for (d) laminar flow, (e) transitional flow, and (f) turbulent flow regimes.

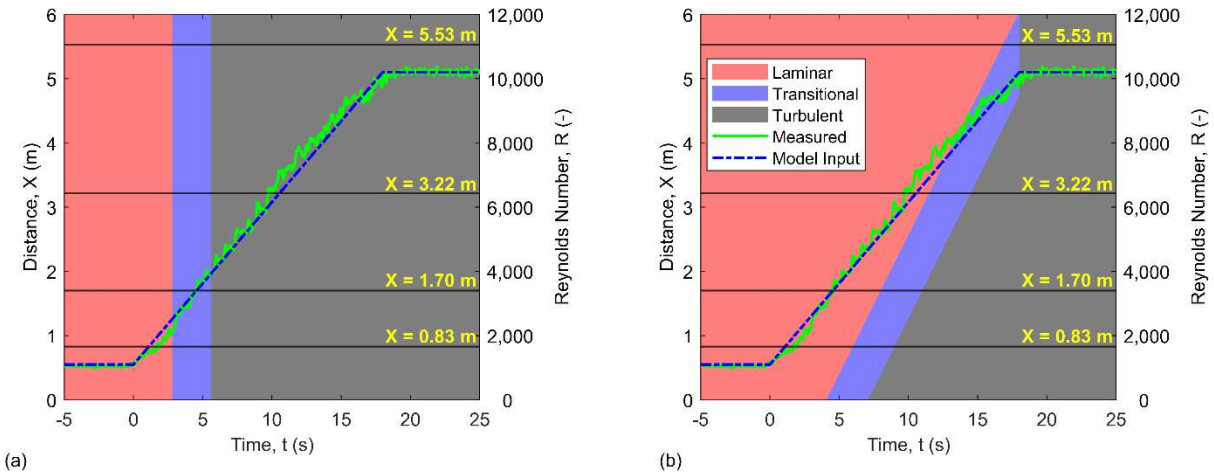

Fig. 9. Mean accelerating flow and laminar, transitional and turbulent flow regimes for (a) Model A - longitudinally uniform transition time; and (b) Model B - longitudinally non-uniform transition time.

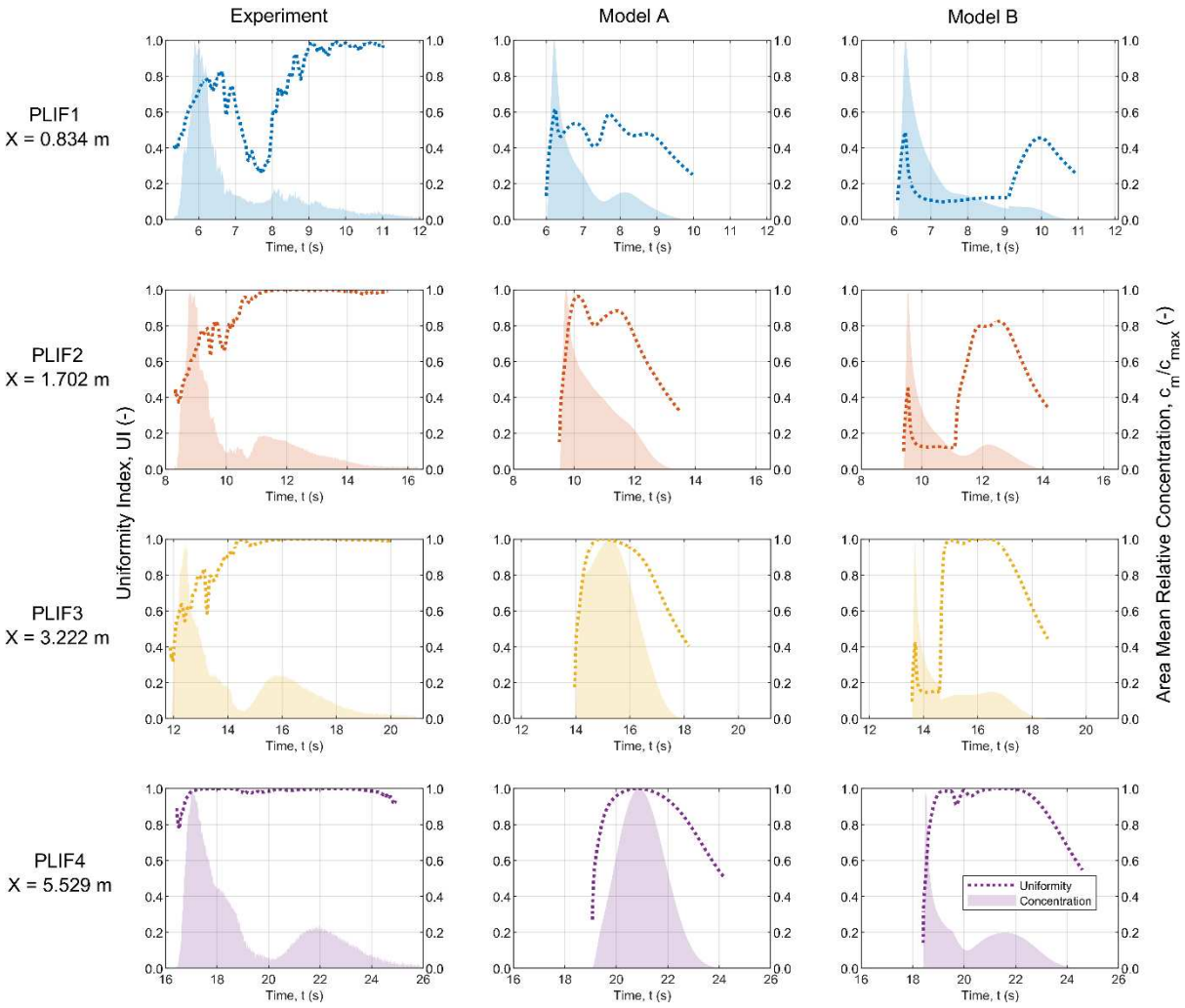

Fig. 10. Experimental and simulated concentration results for Injection at 0 s, R = 1,093.

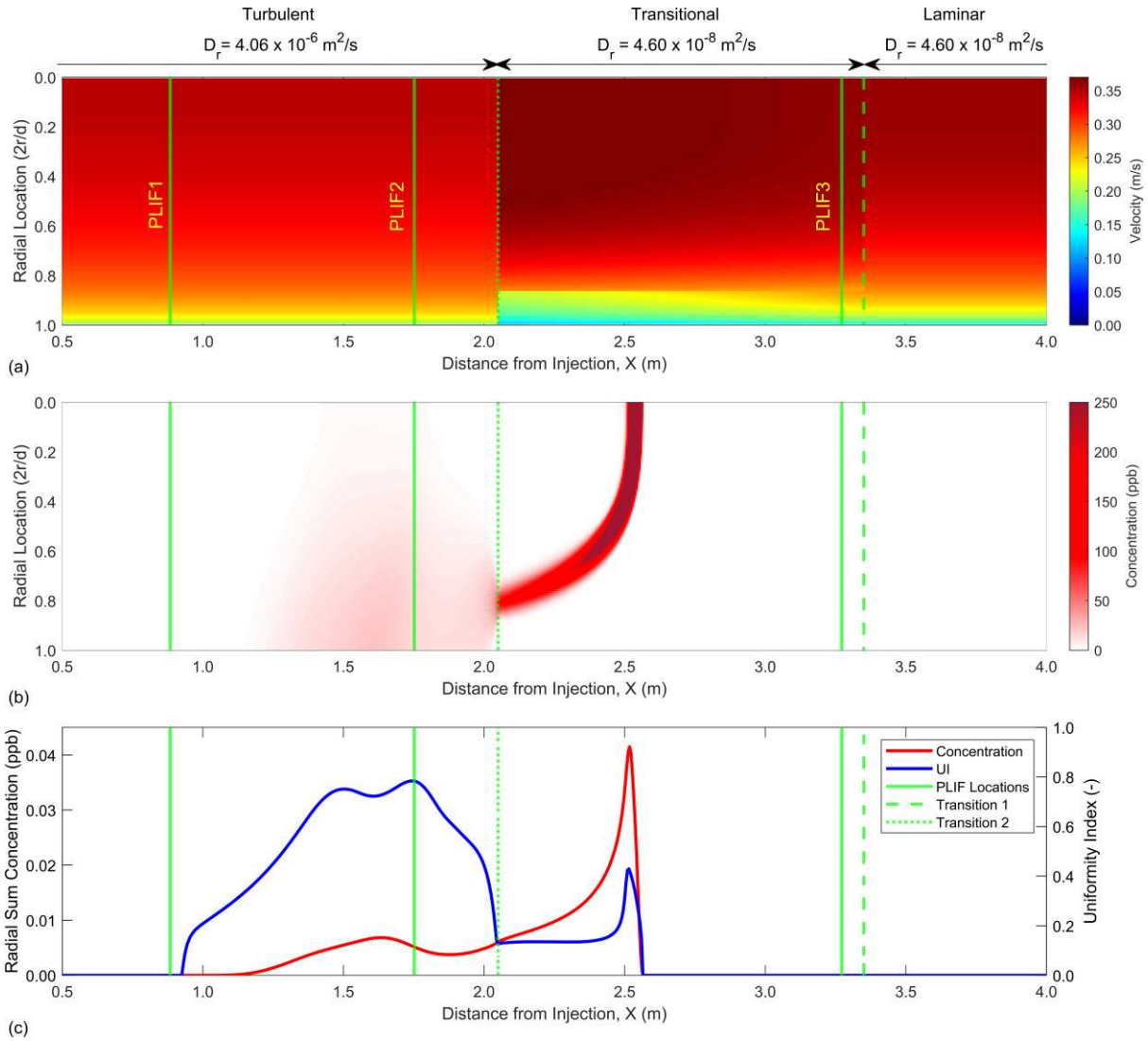

Fig. 11. Simulated (a) velocity, (b) spatial concentration and (c) radial sum concentration at t = 11.8 s, R = 7,066 during the acceleration using Model B.

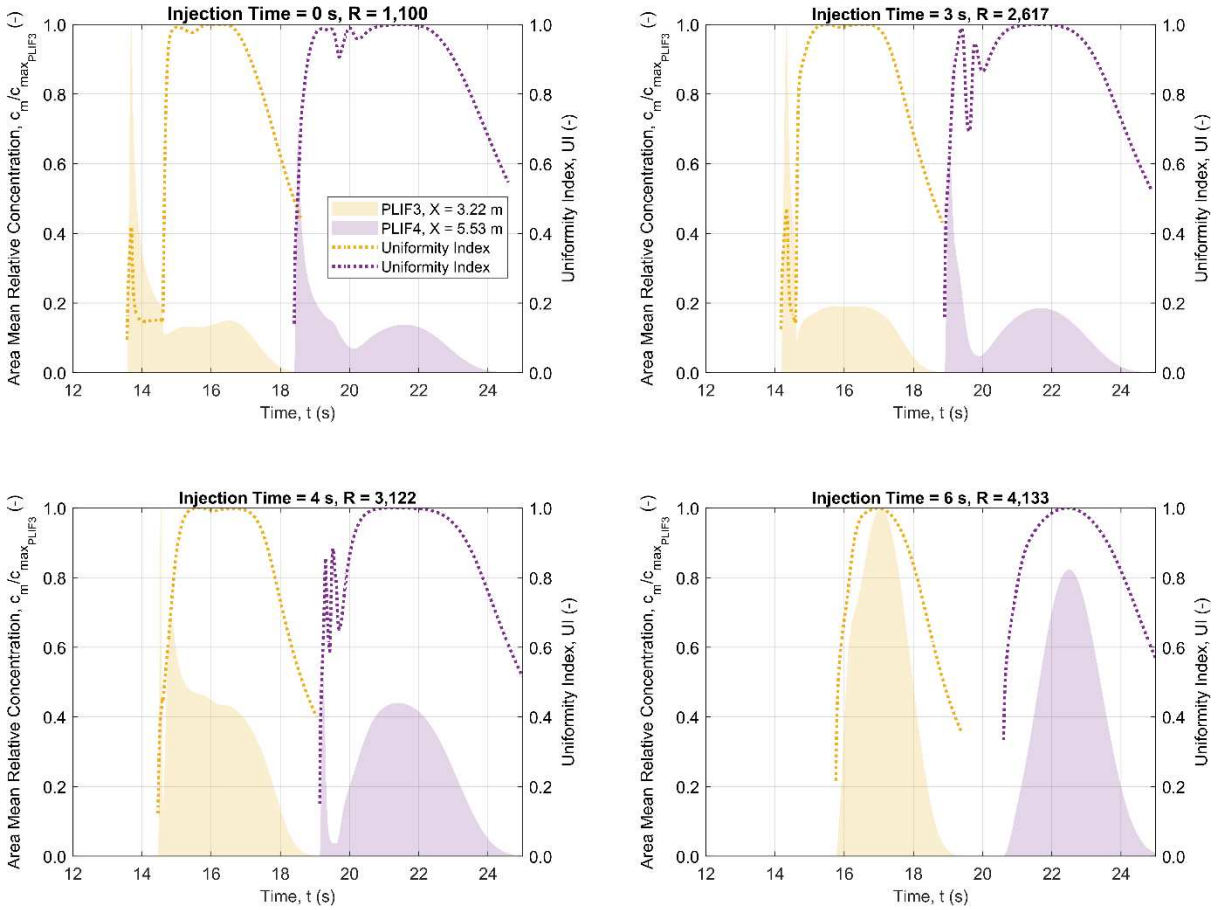

Fig. 12. Simulated concentration and uniformity index for selected injection times at the two downstream locations using Model B.

Table 1. Calibrated parameters for the velocity profiles at different flow regimes.

Flow	m	n	Constant Velocity Region (2r/d)	R^2
Laminar	2.436	4.074	-	0.880
Transitional	4.219	2.281	0.86 – 1.00	0.853
Turbulent	1.644	6.754	-	0.856